Downslope Windstorms in the Front Range: A 21-Year Climatological Analysis

by

Serena Lipari-DiLeonardo

B.S Mathematics, CUNY College of Staten Island, 2018

M.S. Environmental Science, CUNY College of Staten Island, 2020

A thesis submitted to the

Faculty of the Graduate School of the

University of Colorado in partial fulfillment

of the requirements for the degree of

Master of Science

Department of Applied Mathematics

2023

Committee Members:

Julie K. Lundquist, Chair

Ian Grooms

William Kleiber

Lipari-DiLeonardo, Serena (M.S., Applied Mathematics)

Downslope Windstorms in the Front Range:

A 21-Year Climatological Analysis

Thesis directed by Dr. Julie K. Lundquist

A 21-year climatology of downslope windstorms in Boulder, Colorado is derived from data measured by a meteorological tower at the National Renewable Energy Laboratory's Flatirons Campus (formerly the National Wind Technology Center). Downslope windstorms occur regularly in the Front Range, often exacerbating wildfires and causing structural damage. Wind speed, wind direction, and windstorm duration criteria are imposed on meteorological data for classifying downslope windstorm events at a 1-minute and hourly temporal resolution. Windstorm trends are investigated daily, monthly and yearly. Over this period, 1172 downslope windstorms were classified, averaging 56 windstorms per year with a standard deviation of 8.7 windstorms per year. Downslope windstorms were found to exhibit significant seasonal patterns with January being the peak month for downslope windstorm occurrences, as well as windstorm intensity and duration. Annual windstorm frequencies were fit with generalized least squares and generalized linear models to investigate temporal trends between 2002-2022. Annual hours of strong westerly winds as well as sustained 1-minute wind speeds at the 90th, 95th, and 99th percentile all exhibited significant decreases during this period. When applied to MERRA2 reanalysis data, a similar annual trend is observed in the number of windstorm hours, while a contrasting trend is observed in annual windstorm frequency. To the best of our knowledge, this is the first study to classify downslope windstorm events using 1-minute temporal resolution meteorological data east of the Rocky Mountains.

Contents

Chapter

1 Introduction 1

2 The Dataset and Downslope Windstorm Classification 6

2.1 Data sources 6

2.2 Data download and processing 9

2.3 Downslope windstorm classification 9

3 Trend Analysis 12

3.1 Annual trend analysis 12

3.1.1 Linear regression models 13

3.1.2 Generalized linear models 14

3.2 Seasonal trend analysis 15

3.2.1 Deseasonalization and detrending 16

3.2.2 Spectral analysis 16

4 Results 19

4.1 Annual trends 19

4.2 Seasonal trends 22

4.3 Diurnal trends 27

4.4 MERRA-2 reanalysis comparison 27

5 Discussion 30

6 Conclusion 31

Bibliography 33

Tables

Table

1.1 Literature review for downslope windstorm and chinook classification between 1946-2007 5

4.1 Differences by the paired t-test between winter and summer downslope windstorm frequency, mean duration and mean wind speed, and total hours of strong westerly winds. Mean and SD are given as winter, summer. 25

Figures

Figure

1.1 Terrain map of Colorado. The region of interest is the city of Boulder indicated with a red dot, situated where the Rocky Mountains meet the Great Plains. [18] 2

2.1 Map of the NREL Flatirons Campus (M2) with the structures and instrumentation indicated by the symbols described in the legend. The meteorological tower indicated by the green triangle supplied the wind measurements for this work. (Courtesy of Joe Smith and Steve Haymes at NREL) 7

2.2 Wind speed distributions for (a) 2004 and (b) 2020 are depicted using their probability density functions. The wind rose plot for 1-minute sustained wind speeds between 2002-2022 is depicted in (c), where distance from the origin depicts the cumulative frequency of winds in that direction sector. 8

2.3 Visualization of a classified windstorm from February 2022. (a) depicts the wind speed over time, with the green shaded region representing a windstorm event. (b) depicts the wind direction over the course of the wind event, where dark blue markers correspond to westerly wind falling within the threshold bounds. 10

3.1 GLS model fits with a 95% confidence interval via Bootstrapping for (a) windstorm frequency; (b) hours of strong westerly wind; (c) windstorm average duration; (d) windstorm average wind speeds. Plots in the right column display the associated residuals for each of these model fits. 14

3.2 Monthly observations along with the associated spectral analysis for (a) downslope windstorm frequency and (b) downslope windstorm hours. The frequency-power spectrum is depicted for each time series, with the function height representing the power associated with each frequency value. 17

4.1 Annual trends along with their GLS regression fits and p-values associated with the predictor (years). Slope values are in units per year. From top to bottom: (a) downslope windstorm frequency; (b) downslope windstorm hours; (c) time over threshold; (d) mean DW duration; (e) mean DW wind speed; (f) median number of lulls per DW. 20

4.2 Annual downslope windstorm trend fitted with generalized least squares, Poisson and negative binomial regression models along with their p-values associated with the predictor (years). 21

4.3 Annual wind speed (a) 75th, (b) 90th, (c) 95th and (d) 99th percentile trends. . . . 22

4.4 Monthly windstorm frequency distribution. (a) Violin plot showing distribution of windstorms for each month; (b) Bar plot showing average monthly windstorms with standard error along with seasonal trends. 23

4.5 Seasonal trends using monthly data points. Error bars are computed via bootstrapping standard error. (a) Windstorm frequency represents the average number of monthly storms per year; (b) Time over threshold represents the average number of monthly hours of strong westerly winds per year; (c) Windstorm wind speeds represent the mean average wind speed during a windstorm in each month; (d) Windstorm durations represent the mean average windstorm duration in each month. 24

4.6 (a) Annual and (b) seasonal comparisons of windstorm frequency and time over threshold. 25

4.7 Decomposed monthly trends for (a) windstorm frequency and (b) windstorm hours interpolated with monthly data points. Generated via *seasonal_decompose* from the statsmodels package. 26

4.8 (a) Monthly windstorm frequency and (b) monthly windstorm hours overlaid with deseasonalized smoothed filter functions. By applying a moving-window convolutional filter with a frequency of 12, we effectively disregard the seasonal cycle to infer an interpolated underlying trend, plotted in teal. 26

4.9 Diurnal distributions of (a) windstorm start times, (b) end times, and (c) overall windstorm temporal distribution. Heights are computed as probability values. 28

4.10 Comparison of results using observations and MERRA-2 reanalysis data for (a) DW frequency, (b) DW hours; (c) mean DW wind speed; and (d) mean DW duration. Correlations are assessed with Pearson's r for (a) and (b) whereas (c) and (d) are assessed with Spearman's r. 29

Chapter 1

Introduction

Downslope windstorms can cause significant damage to communities and infrastructure [2, 7, 19, 40], and can intensify the impacts of regional wildfires such as the Marshall fire of December 2021, which quickly became the most destructive wildfire in Colorado history [6, 7, 23]. Turbulence associated with downslope windstorms additionally creates hazardous conditions for aircraft, such as the case in December 1992 where turbulence during a downslope windstorm resulted in a DC-8 cargo jet making an emergency landing due to losing an engine and part of a wing [9, 27, 32].

These extreme wind events occur across the globe, with local names such as the Rocky Mountain chinook [29], the Alpine foehn [34], the southern Californian Santa Ana [33, 39], the Croatian bora [16], and the Argentine zonda [28]. Collectively, these winds are referred to as downslope winds, capable of gusting above hurricane force (34 m s^{-1}) [19]. Many downslope wind events are characterized by a rapid warming of the air as it descends – referred to as the "Foehn effect" – while downslope windstorms as a whole do not necessarily involve a significant temperature change [4, 14].

In Colorado, the Rocky Mountains are elongated from north to south with summits at heights of 1500 to 2100 m above the adjacent plains, equivalent to heights of 1800 to 4400 m above sea level [22]. Figure 1.1 shows the terrain of Colorado with the city of Boulder situated just at the foothills of the Rocky Mountains. As Boulder is located on the lee side of the mountain range, downslope windstorms regularly occur and have been responsible for structural damage and historical wildfires.

Despite the importance of windstorms to the Front Range, there are no climatologies assessing

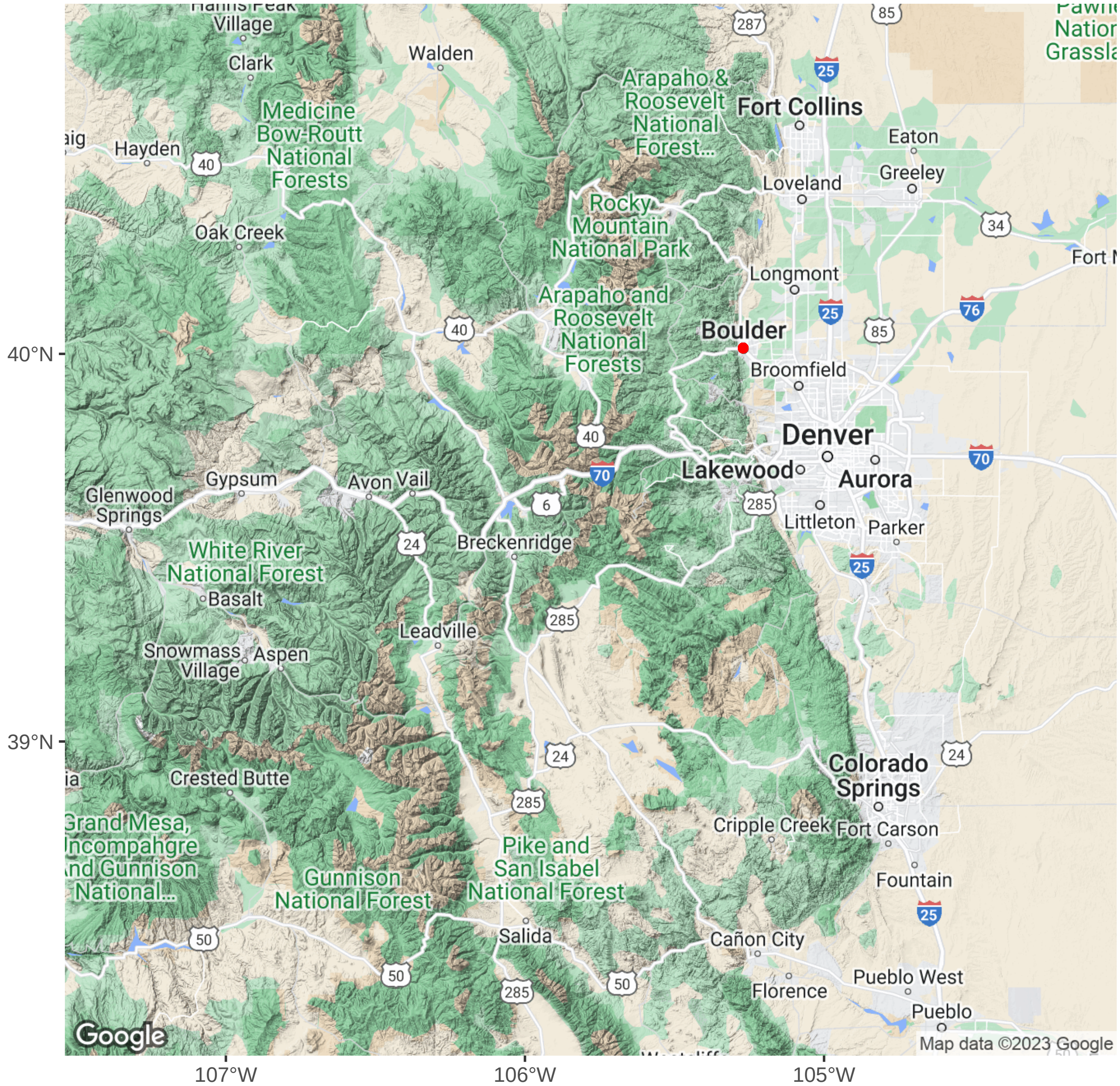

Figure 1.1: Terrain map of Colorado. The region of interest is the city of Boulder indicated with a red dot, situated where the Rocky Mountains meet the Great Plains. [18]

how windstorms have locally changed over the last few decades. Methodologies for classifying downslope windstorms have evolved throughout the years with detailed surface wind observations appearing in the 1970s [19]. Two major climatologies of downslope windstorms in the Boulder area were performed in [4] and [40]. The climatology in [40] is based on newspaper accounts spanning

151 windstorms occurring between 1869 and 1972, where windstorms are classified based on general properties (high wind speeds, extreme gustiness, and pauses in wind activity) as well as areal extent and damage severity. The analysis in [4] classified and investigated 20 windstorm events over three winters, where a windstorm period was defined as one during which maximum speeds exceeded 22 m s^{-1} with at least one station recording a gust over 32 m s^{-1}.

More recent analyses have been performed outside of the Boulder area for classifying windstorms, e.g. [37] propose a self-organizing map (SOM) algorithm to classify downslope windstorms by synoptic pattern into three representative types, and [1] use a model involving cross-barrier wind speed, near-mountain top static stability, and downward vertical velocity. As a downslope windstorm is a localized mesoscale weather system forced by synoptic-scale airflow, much work has been done in analyzing large-scale, mesoscale and turbulent-scale features important for windstorm development, e.g. [4, 19, 20, 37].

Defining criteria for downslope windstorms is difficult due to the absence of an explicit and well-established definition. While much of the early work on downslope windstorms and chinooks emphasized thermal effects, more recent research has placed an additional focus on wind intensity (Table 1). Given this distinction, we do not refer to downslope windstorms in this study indiscriminately as chinook events, as we only consider wind speed and direction in our classification as in [4]. Furthermore, as several studies on downslope windstorms have only included winter months (DJF) in their work, these differences pose a difficulty in directly relating the results of previous climatologies with the results found here.

In this study, we present a climatology of downslope windstorms in the Front Range for the period 2002–2022 to better understand their characteristics and diurnal, annual, and seasonal distributions. Additionally, this paper provides a methodology for classifying windstorm events using high temporal resolution meteorological data. Hours of strong westerly winds are used as an additional metric to compare with windstorm counts to better understand not only how the frequency of windstorms have been changing, but additionally how the winds associated with windstorm events have been changing. First, we classify downslope windstorms using wind speed and direction observations, and then we fit the windstorm data with linear and generalized linear regression models to assess annual trends and examine to what extent downslope windstorms have changed over time in terms of overall frequency, intensity and duration. Windstorm distributions are also investigated seasonally, monthly and diurnally over this time period. By analyzing windstorm trends, we aim to provide new insights into the recent climatology of downslope windstorms in the Boulder area of the Rocky Mountains, and to inform the development of risk management strategies and mitigation efforts.

Wind Speed	Duration	Wind Direction	Temperature	Properties	Altitude *(AGL) **(ASL)	Source
		SW	Warm for the season	Dry		Thiessen 1946
		W	Warm	Dry		Cook and Topil 1952
			Max temp > 40 degrees (only DJF)			Longley 1967
		WNW, W, WSW		Fohn nose present		Brinkmann 1970
Max hourly > 22 m s^{-1}				Gust(s) > 33 m s^{-1} (hurricane force)	3.4m*	Brinkmann 1974
Constant mean > 20 m s^{-1}		WNW		Gust(s) > 34 m s^{-1} Waves of horizontal wavelength of order 50-100km	0.5km**	Klemp and Lilly 1974
High	Several hours to several days; Average 8h	W		Generally no precipitation Generally during cold season Cloudy or partly cloudy with high and middle level clouds Extreme gustiness		Whiteman and Whiteman 1978
> 4.5 m s^{-1}	> 1h		Daily max temp > long-term monthly mean max temp			Golding 1978
Unusually strong		W	Warm	Dry		Mathai et al 1980
> 4.5 m s^{-1}		SSW to WNW	Eventual mean daily value > daily normal	Drop in relative humidity	2m*	Nkemdirim 1990
> 4.5 m s^{-1}	1h	SSW to WNW	Eventual daily max > daily normal	Drop in relative humidity	600-1600m**	Nkemdirim 1996
> 18 m s^{-1}		WSW to NNW		Gusts > 35-50 m s^{-1}	15m* 700hPa**	Mercer et al. 2007

Table 1.1: Literature review for downslope windstorm and chinook classification between 1946-2007

Chapter 2

The Dataset and Downslope Windstorm Classification

2.1 Data sources

The temporal and wind data used in this study consist of records from an instrument mounted at 10m on an 82m meteorological tower at the National Renewable Energy Laboratory's Flatirons Campus located in Colorado's Front Range, depicted in Figure 2.1. Wind speed (m s^{-1}) and wind direction (degrees) data were acquired from 1 Jan 2002 through 31 Dec 2022 (21 years totaling 7665 days). The tower is located approximately 8km south of Boulder, Colorado at latitude 39.9106° North and longitude 105.2347° West with its base at an elevation of 1855m above mean sea level (MSL). Readings were taken every two seconds and averaged over one minute. (Data attributed to Jager and Andreas 1996)

Figure 2.2 serves to describe the wind speeds and wind directions characteristic of this dataset. Wind speeds take on an approximately Weibull distribution, with lower wind speeds being the most frequent. Figure 2.2c illustrates how the wind speed and direction are distributed at this location, where the length of each 20° ”spoke” around the circle indicates the amount of time that the wind blows from that particular direction. Sustained 1-minute winds at the M2 site most frequently blow from the WNW direction. Particularly, stronger winds (> 8.6 m s^{-1}) almost exclusively have a westerly component, indicating that nearly all high-speed winds in the area originate from the west.

Additionally, MERRA-2 reanalysis data are used for comparison of results with the observational data to assess whether the reanalysis data are capturing downslope windstorm trends. The

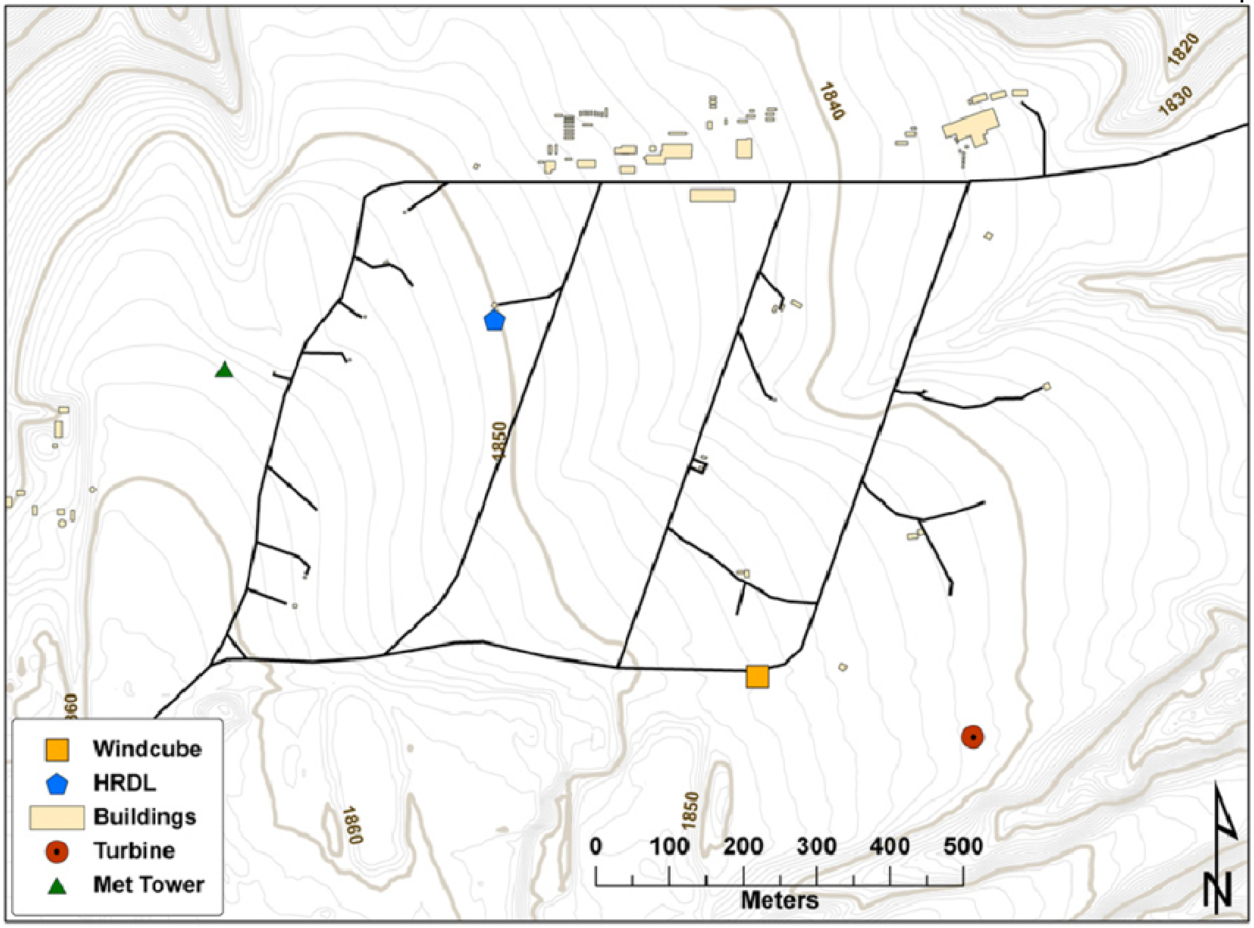

Figure 2.1: Map of the NREL Flatirons Campus (M2) with the structures and instrumentation indicated by the symbols described in the legend. The meteorological tower indicated by the green triangle supplied the wind measurements for this work. (Courtesy of Joe Smith and Steve Haymes at NREL)

MERRA-2 dataset is generated using a sophisticated data assimilation system combining observations from various sources, including satellites, radiosondes, and surface weather stations, with a numerical weather prediction model to produce a consistent and high-quality record of atmospheric conditions [25]. MERRA-2 data comes from NASA's Global Modeling and Assimilation Office (GMAO), and is the second generation of the Modern-Era Retrospective analysis for Research and Applications (MERRA) dataset covering the period from 1980 to the present. Hourly averaged wind data from MERRA-2 and observations used for comparison span 1 Jan 2002 through 31 Dec 2020. For the most accurate comparison, the reanalysis data are downloaded at the same height

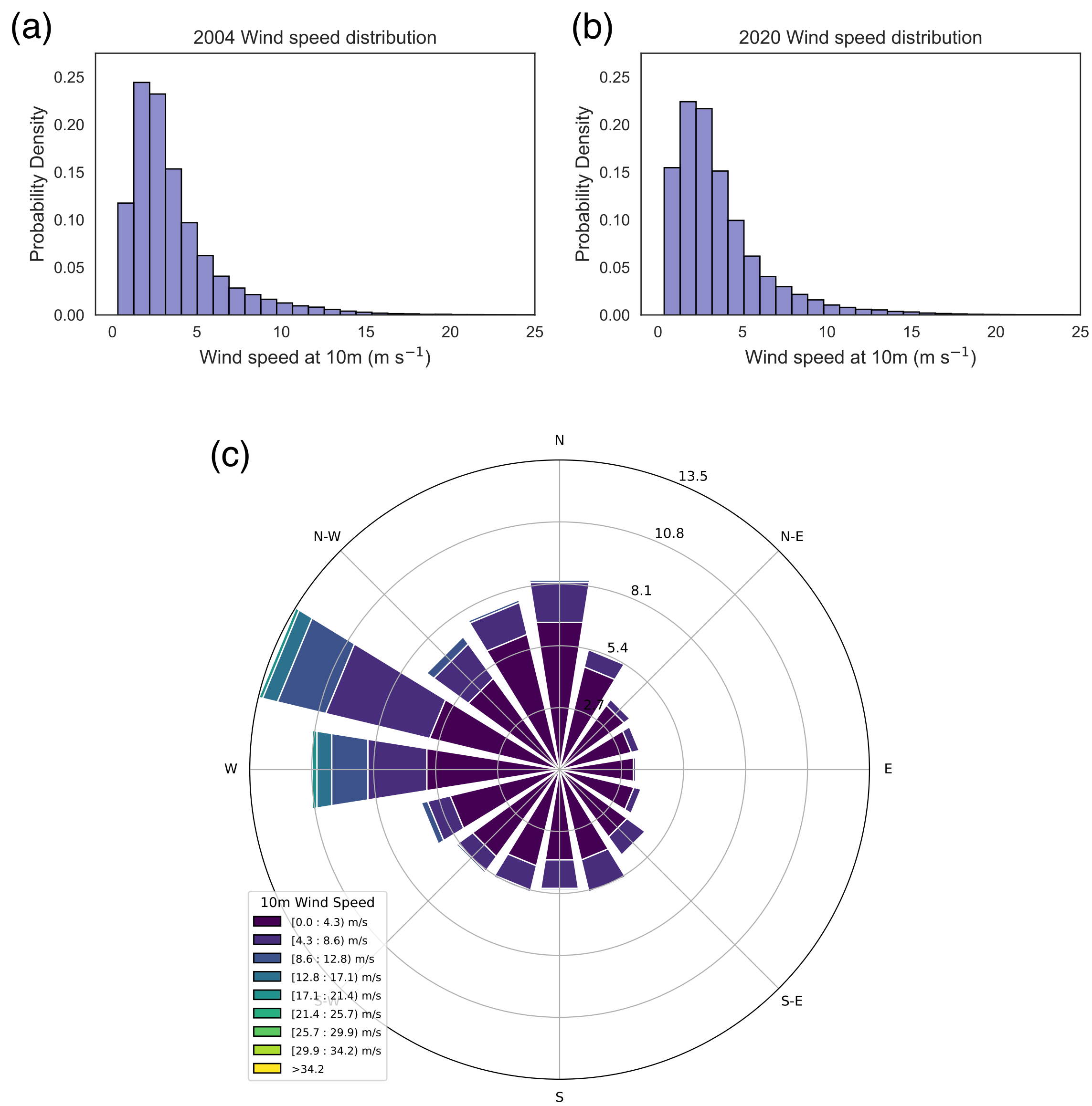

Figure 2.2: Wind speed distributions for (a) 2004 and (b) 2020 are depicted using their probability density functions. The wind rose plot for 1-minute sustained wind speeds between 2002-2022 is depicted in (c), where distance from the origin depicts the cumulative frequency of winds in that direction sector.

and coordinates as the observational data, specifically 10m wind data at latitude 39.9106° North and longitude 105.2347° West.

2.2 Data download and processing

Data was downloaded yearly using the MIDC raw data API (`https://midcdmz.nrel.gov/apps/data_api_doc.pl`) as csv files. First, a subset of desired values was specified for analysis (year, day of year (DOY), average wind speed at 10m, average wind direction at 10m), as the API data download includes all raw data by default. Then the specified data was read into python and stored as a *DataFrame* through pandas, an open source data analysis and manipulation tool. Any values of −99999.0 were replaced with NaN values to avoid including inaccurate data in the analysis. A function converting the day of year to a date was applied to each row in the DOY column, and these dates were then converted into python *DateTime* objects for an effective and unambiguous representation of dates.

Hourly averaged observational data are used for downslope windstorm classification and the subsequent comparison as the reanalysis data are available as hourly averages. MERRA-2 wind data at a height of 10m was accessed from `www.renewables.ninja` [30, 38]. Notably, this dataset does not include wind direction measurements, thus the classifications used for comparison involve only wind speed. As the majority of winds, particularly strong winds, originate from the west as illustrated in Figure 2.2c, this impact is not considered to be significant in the identification of downslope windstorm events.

2.3 Downslope windstorm classification

The criteria used for identifying downslope windstorm (DW) events are: (1) wind speeds greater than 4.5 m s^{-1}; (2) sustained westerly winds, specifically between $285° \pm 45°$; (3) breaks or lulls in (1) or (2) last fewer than 12h; (4) the DW event wind speed averages must satisfy (1); and (5) DW events last at least 1h. The wind direction bounds are centered around 285° as that was recorded as the most frequent wind direction at the site [11]. Lull periods where the wind speed or wind direction fall out of range are limited to 12h following [3] and [40]. An illustrated example of a windstorm event using our criteria is presented in Figure 2.3.

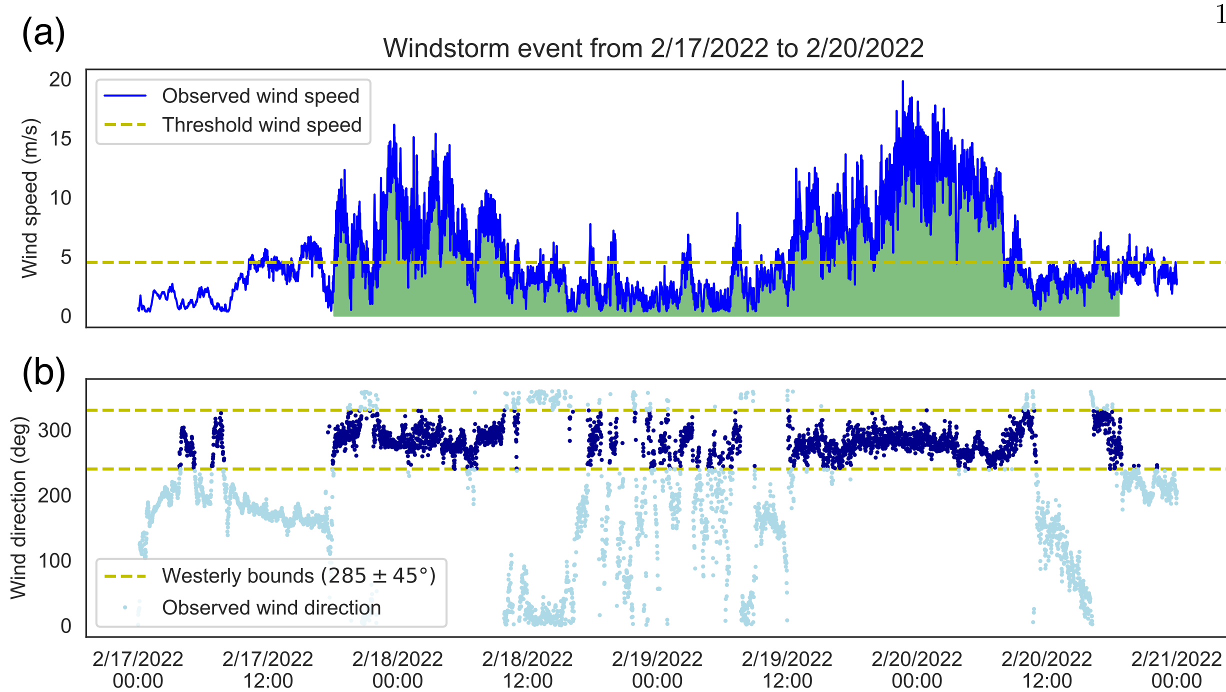

Figure 2.3: Visualization of a classified windstorm from February 2022. (a) depicts the wind speed over time, with the green shaded region representing a windstorm event. (b) depicts the wind direction over the course of the wind event, where dark blue markers correspond to westerly wind falling within the threshold bounds.

Once the data are loaded and cleaned and classification criteria is established, windstorm events can be classified. To attribute properties to windstorm events for accessibility, windstorm objects were created as a data class defined by a start and stop index. The wind speeds and wind directions are then used as inputs to a filtering function, along with their specified threshold values, which returns windstorms within a time series. The function works by iterating through every minute to determine whether or not the wind meets the classification criteria to be considered a windstorm. When the wind speed and direction meet the criteria, a flag is raised that a windstorm has begun. If either ceases to meet the criteria, a lull begins. If that lull period exceeds the specified duration, however, that entire event is disregarded, unless the period before the lull was long enough to be considered a windstorm event itself. Otherwise, if the wind speed and direction begin to satisfy the windstorm criteria before the maximum lull duration is reached, then that period is indeed considered a lull and the windstorm status remains true. Figure 2.3 illustrates an example of a windstorm event with a lull period, where thresholds are not met for a period of time before rising above threshold again. This method is performed on each entire year's time series, where the total number of windstorms and their properties are logged.

The wind speeds and directions during each windstorm, the times during which each windstorm occurred, and the lulls that occurred during that windstorm are all recorded as properties of that windstorm. Periods where the wind speed or direction falls outside of the specified threshold values for less than a specified period of time are considered to be lulls. This works to prevent a windstorm from being considered finished if, for example, the wind speed dips below threshold for a short period of time and then picks back up. Lulls were also constructed as a data class defined by a start and stop index, along with their duration as a property. To summarize, each windstorm's properties of wind speed and direction during the length of the storm, total duration and lulls–each with their own duration–are made easily accessible.

Chapter 3

Trend Analysis

3.1 Annual trend analysis

Linear and generalized linear regression models are used to assess whether connections exist between time and the annual trends of DWs and DW properties. After ensuring assumptions are met and implementing the appropriate models, we can compare their performances via log-likelihood values, where higher values are associated with a better model fit. Additionally, the total time spent meeting wind speed and direction classification criteria is used as a comparison metric. This provides a means to verify whether the frequency of windstorms follows the same trend as the amount of strong westerly winds. The time spent satisfying thresholds for a time series is computed by iterating over the wind speed and direction at each minute and adding one to a counter if wind speed and direction fit the windstorm criteria for that minute. This was computed annually and logged for trend analysis, where it will be referred to as "time over threshold".

We also investigate whether the occurrence of extreme winds has been changing over this period through the Mann-Kendall test for trends. First, we compute the 75th, 90th, 95th and 99th percentile 1-minute wind speeds for each year and then plot each of their trends as a time series. A two-tailed Mann-Kendall test is then used to test whether extreme winds have been changing in time at the 95% confidence level. This test measures monotony of the trend, represented by the parameter τ. Notably this test does not require the data to be parametric or linear, but assumes no auto-correlation, i.e. that the variable is not correlated with a time-lagged copy of itself. While 1-minute wind speeds can be subject to high auto-correlation, annual wind speeds retain virtually no coherent memory (e.g. [35]).

3.1.1 Linear regression models

When the assumptions of OLS (ordinary least squares) hold, it is the best linear unbiased estimator as a result of the Gauss-Markov theorem. One assumption for OLS is homoscedasticity, or homogeneity of variances. White's Test is used to determine if heteroscedasticity is present in the annual windstorm frequency data, resulting in a test statistic $X^2 = 6.165$ with a p-value of $p = 0.046$. Since $p < 0.05$, we have sufficient evidence to reject the null hypothesis that homoscedasticity is present, i.e. that residuals are equally scattered for the OLS model. The alternative we use here is generalized least squares (GLS), which takes into account the inequality of variance in the observations. The assumptions for GLS are similar to those of OLS without the homoscedasticity requirement, specifically 1. there is a linear relationship between the response and predictor variables, 2. the errors are independent, and 3. the responses are normally distributed. Under these assumptions, linear regression via GLS (generalized least squares) is applied to fit the annual trend data for DW frequency, DW properties, and hours of strong westerly winds. Average DW wind speed, average DW duration and hours of strong westerly winds are continuous variables with normally distributed GLS residuals, as depicted in Figure 3.1.

As an assumption for linear models is normally distributed residuals, we first test this condition for each variable via the Shapiro-Wilk test. The GLS model results in test statistics of: (1) $W = 0.98$ with an associated p-value of $p = 0.93$ for annual windstorm frequency, (2) $W = 0.97$ with an associated p-value of $p = 0.70$ for hours of strong westerly winds, (3) $W = 0.97$ with an associated p-value of $p = 0.82$ for average windstorm duration, and (4) $W = 0.96$ with an associated p-value of $p = 0.52$ for average windstorm wind speed. As each of these are greater than $\alpha = 0.05$, we conclude at the 95% confidence level that the residuals for each variable associated with the GLS model follow a normal distribution, and thus the requirements for linear modeling are satisfied.

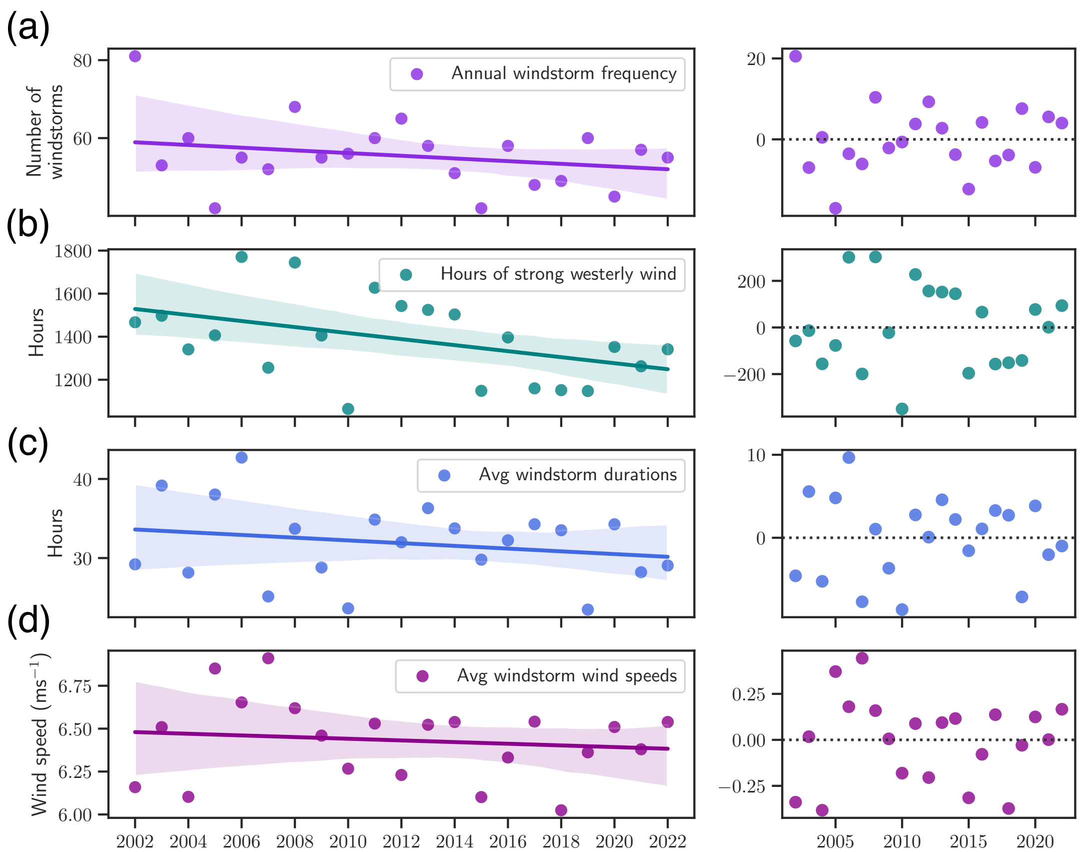

Figure 3.1: GLS model fits with a 95% confidence interval via Bootstrapping for (a) windstorm frequency; (b) hours of strong westerly wind; (c) windstorm average duration; (d) windstorm average wind speeds. Plots in the right column display the associated residuals for each of these model fits.

3.1.2 Generalized linear models

The number of annual DWs are discrete count data representing the number of DW events occurring during a fixed period, making DW annual frequency suitable for count data models such as Poisson and negative binomial regression. For these two models, we assume that DW events occur independently and randomly for each year with a known average. The Poisson model has the properties that the mean is $E(Y) = \lambda$ and the variance is $Var(Y) = \lambda$ which implies equidispersion of the data. Appropriateness of the Poisson model is first assessed by testing for overdispersion, i.e.

whether $Var(Y) > E(Y)$. We test this assumption as a null hypothesis that $Var(Y) = \lambda$ against the two-sided alternative where the variance is of the form $Var(Y) = \lambda + cf(\lambda)$ where the constant $c < 0$ implies underdispersion and $c > 0$ implies overdispersion, and the function $f(\lambda)$ is some monotonic function of the mean. For this test, $f(\lambda)$ is specified as a linear function. The function *dispersiontest* from the R package AER was used to run this test as in [5]. The resulting statistic is $z = 0.444$ with a p-value of $p = 0.657$, and the constant c is estimated to be approximately $c = 0.168$. Since $p > 0.05$, we fail to reject the null hypothesis at the 95% confidence level that there is equidispersion in the annual number of downslope windstorms. Therefore, by this test, the Poisson model is appropriate in this case.

The negative binomial model is widely promoted as an alternative to the Poisson model due to the potential for overdispersion due to individual counts being more variable than is implied by the model, which may produce misleading inferences (e.g. [15, 17, 26]) and will additionally be used here to fit annual windstorm frequency. The negative binomial model has the properties that the mean is $E(Y) = \lambda$ and the variance is $Var(Y) = \lambda + \alpha\lambda^2$ where α is the dispersion parameter. Note that the case of $\alpha = 0$ produces the Poisson model.

3.2 Seasonal trend analysis

Aside from discerning an overall trend in time, it's also valuable to investigate the existence of seasonal trends in windstorm events. The data was grouped by months rather than years, and the monthly time series data was run through our classification function. This produced a windstorm frequency for each month. Grouping the months by season (DJF, MAM, JJA, SON) additionally reveals seasonal variability in the occurrence of downslope windstorms. Bar plots and violin plots are used to illustrate the distribution of monthly windstorms in Section 4. Error bars for the bar plots represent standard error constructed via bootstrapping, as the number of monthly windstorms in four out of twelve samples failed the Shapiro-Wilk test and thus were found to be non-parametric. Bootstrapping was conducted with $9,999$ resamples using the bias-corrected and accelerated (BCa) bootstrap interval, which corrects for bias and skewness in the distribution of bootstrap estimates. The standard error is calculated as the standard deviation of the bootstrap distribution. After error bars are constructed, we will be able to test for a significant seasonal cycle, i.e. test the seasonal distribution of windstorms against a uniform distribution using the chi-square goodness-of fit test. We choose the chi-square test as it is applicable to discrete distributions, unlike the Anderson-Darling and Kolmogorov-Smirnov goodness-of-fit tests which are intended for continuous distributions.

3.2.1 Deseasonalization and detrending

We run the algorithm on monthly data to acquire windstorm frequencies at the monthly resolution in order to assess downslope windstorm seasonal variations. The monthly windstorm frequency time series consisting of 252 data points is decomposed into three components: trend, seasonality, and residuals, using an additive model through *seasonal_decompose* from the statsmodels package. First, the trend is estimated by applying a convolution filter to the number of monthly windstorms, i.e. a centered moving average is applied to the time series. This effectively smooths the data to illustrate the trend with less variability. To calculate the seasonal component, the computed trend is first removed from the original series, then the series is split at every 12 months and averaged to attain the seasonal trend which is extrapolated to the full time series. The residual component is what remains after removing the trend and seasonal components from the original series.

3.2.2 Spectral analysis

Downslope windstorms exhibit a strong seasonal cycle, as illustrated in Figure 3.2 and discussed further in Section 4. Spectral analysis is a method for analyzing the frequencies and amplitudes present in a signal, here being the occurrence of downslope windstorms and the number of windstorm hours per month. We use this method to identify any recurring patterns in the data corresponding to temporal cycles.

First, for the purposes of significance testing, we construct a synthetic red noise time series to

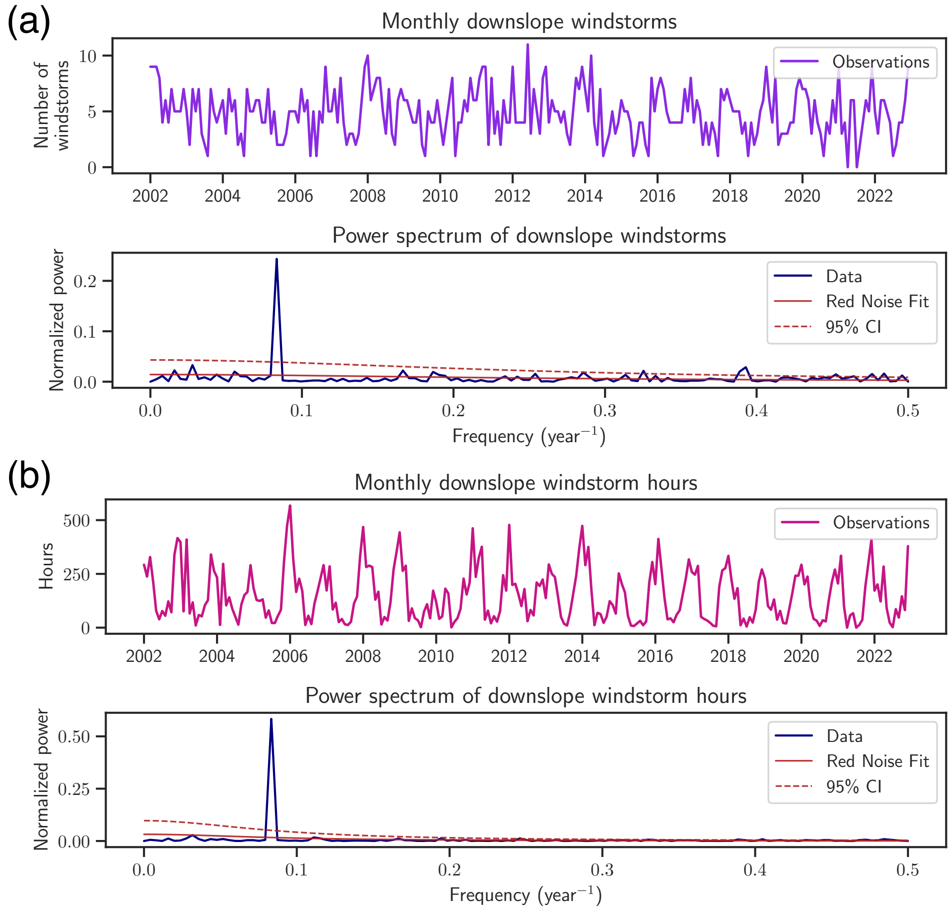

Figure 3.2: Monthly observations along with the associated spectral analysis for (a) downslope windstorm frequency and (b) downslope windstorm hours. The frequency-power spectrum is depicted for each time series, with the function height representing the power associated with each frequency value.

represent the correlation between adjacent data points. Unlike white noise which has no correlation between adjacent data points, red noise has a long-term memory that is incorporated into its auto-correlation function and persists over a range of timescales. The continuous red noise power spectrum function is used to compare against the power spectrum of the observed data, and is represented by the equation:

$$\Phi(\omega) = \frac{2T_e}{1 + \omega^2 T_e^2} \tag{3.1}$$

where T_e is the e-folding timescale of the real data, or the timescale for a quantity to decrease to $1/e$ of its previous value, and ω is the radial frequency. Then, using a 95% confidence interval constructed with the normalized red noise power spectrum, we test the null hypothesis that there is no correlation or pattern in the data beyond what can be attributed to random fluctuations or noise in our observed data. If the observed data fall outside the distribution of the synthetic red noise time series, we can reject the null hypothesis and conclude that the time series exhibits significant correlation or pattern beyond what can be attributed to random fluctuations.

We can see in Figure 3.2 that for both monthly windstorm frequency and monthly windstorm hours, there is a significant peak corresponding with the annual cycle, $\omega = \frac{1}{12} \approx 0.083$, with the peak heights indicating that the seasonal cycle explains approximately 24% of the variance in monthly downslope windstorms, and 58% of the variance in monthly downslope windstorm hours. The remaining frequencies are responsible for less than 5% of the variance and are disregarded.

Chapter 4

Results

4.1 Annual trends

Downslope windstorms have been classified between 2002 and 2022 based on wind data at a 1-minute temporal resolution. This analysis reveals a long-term trend coupled with a distinct annual cycle and little diurnal variability. We assess the annual trends of windstorm frequency, annual windstorm hours as well as total hours of strong westerly wind, and average windstorm properties (windstorm duration, windstorm wind speed, and number of lulls per storm) as depicted in Figure 4.1. It is important to investigate windstorm property trends such as duration and the average number of lulls per storm to consider the potential impact on windstorm frequency.

The least squares linear regression model for each variable is characterized by a negative slope, however only the hours of strong westerly winds are found to have a significant linear relationship with time in years. Figure 4.1a depicts the annual frequency of downslope windstorms, which have a mean of 56 windstorms and standard deviation of 8.2 windstorms. The slope of the line of best fit is -0.382 windstorms per year, representing a decrease of about one windstorm every three years.

Figure 4.1b depicts the annual number of windstorm hours, having a mean of 1799 hours and standard deviation of 8.2 hours. The slope of the line of best fit is -21.9 hours per year, indicating a decrease by about 22 hours of windstorms per year.

Figure 4.1c depicts the annual number of hours of strong westerly winds, having a mean of 1385.9 hours and standard deviation of 194.5 hours. This linear trend is significant at the 95% confidence level with a p-value of 0.046, indicating that there is a significant relationship between

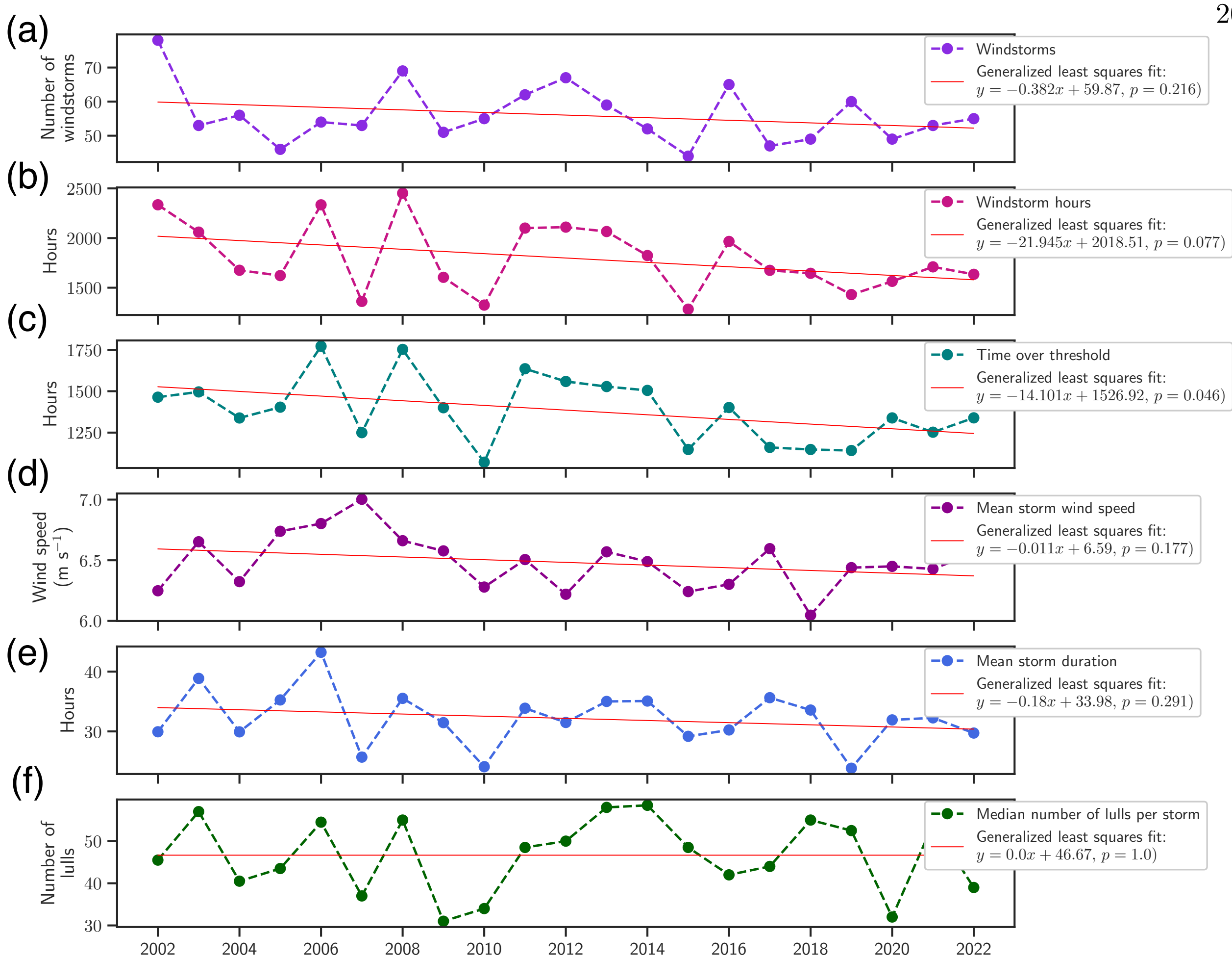

Figure 4.1: Annual trends along with their GLS regression fits and p-values associated with the predictor (years). Slope values are in units per year. From top to bottom: (a) downslope windstorm frequency; (b) downslope windstorm hours; (c) time over threshold; (d) mean DW duration; (e) mean DW wind speed; (f) median number of lulls per DW.

time and the occurrence of strong westerly winds. The associated slope indicates a decrease by about 14 hours of strong westerly winds per year.

Figure 4.1e depicts annual mean windstorm wind speed, which had a mean of 6.5 m s^{-1} and a standard deviation of 0.22 m s^{-1}. The slope of the line of best fit is -0.01 m s^{-1} per year, corresponding to a decrease of about 0.15% average windstorm wind speed per year. Figure 4.1d depicts annual mean windstorm duration, which had a mean of 32.2 hours and a standard deviation of 4.5 hours. The slope of the line of best fit is -0.18 hours per year, corresponding to a decrease in windstorm duration of about 11 minutes per year. Lastly, Figure 4.1f depicts annual average number of lulls per windstorm, having a median of 48.5 lulls and standard deviation of 8.5 lulls. The line of best fit indicates a decrease of about one lull every three years. Lull trends were assessed to ensure that a potential decrease in windstorm durations could not be falsely attributed to an increase in lull occurrences. Note that a lull event lasts at least one minute, and the median lull duration was 9.7 minutes with a standard deviation of 0.7 minutes, or 42 seconds.

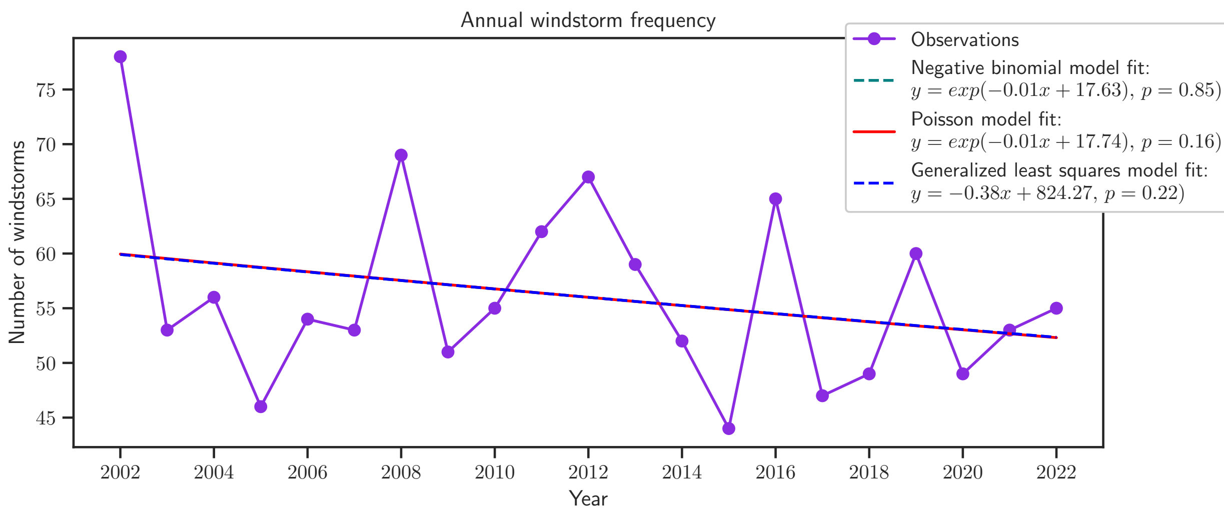

Figure 4.2: Annual downslope windstorm trend fitted with generalized least squares, Poisson and negative binomial regression models along with their p-values associated with the predictor (years).

To assess the model performance for annual windstorm frequency, we compare log-likelihood values associated with each model. The log-likelihood value for the GLS model is -73.122, for the negative binomial model is -105.72, and for the Poisson model is -73.675, indicating that the Poisson model better fits the data in this case, performing just slightly better than the GLS model.

While windstorm average wind speeds have not significantly decreased, the 90th, 95th, and 99th percentile 1-minute wind speeds during this period have all decreased significantly by the Mann-Kendall trend test at the 95% confidence level. Figure 4.3 illustrates annual extreme wind speeds at the 75th, 90th, 95th and 99th percentiles, where wind speed values are one-minute averages in m s^{-1}. Through this test, we conclude that significant negative trends were found for the 90th, 95th and 99th percentile wind speeds, indicating that extreme winds have been decreasing over the period 2002-2022.

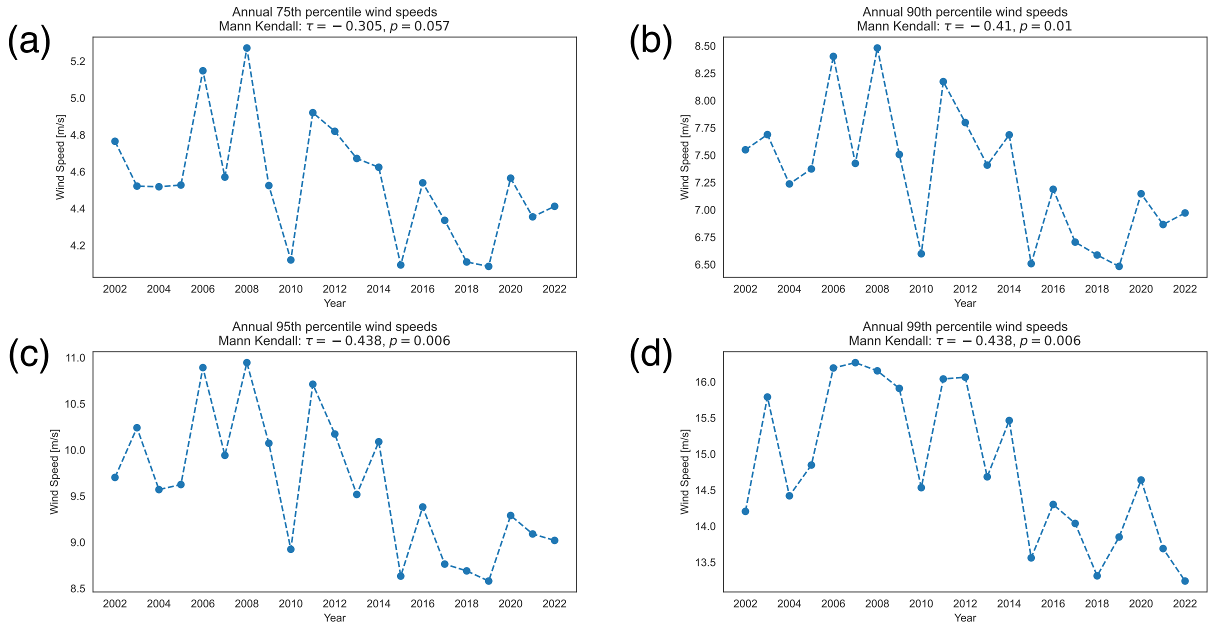

Figure 4.3: Annual wind speed (a) 75th, (b) 90th, (c) 95th and (d) 99th percentile trends.

4.2 Seasonal trends

A strong seasonal cycle emerges in the monthly windstorm data (Figure 4.5). Windstorms are not only less frequent in the summer months than winter months (Figure 4.5a), but also less intense (Figure 4.5c) and shorter (Figure 4.5d). While the number of windstorms appears high in the spring and early summer months (Figure 4.5a), the low recorded hours of strong westerly winds (Figure 4.5b) during that time indicate that these windstorms are shorter in duration. Downslope windstorms between 2002 and 2022 in Boulder, CO have been most abundant in the winter months, coinciding with seasonally strong and persistent westerly flow and high MSLP gradients [1, 7, 10, 40]. Particularly, the most windstorms were observed in the month of January, averaging 6.38 ± 0.4 windstorms each January. DW frequency in December was similar, with an expected value of 6.33 ± 0.38 windstorms each year. July was found to have the fewest windstorms, averaging 2.71 ± 0.27 each year.

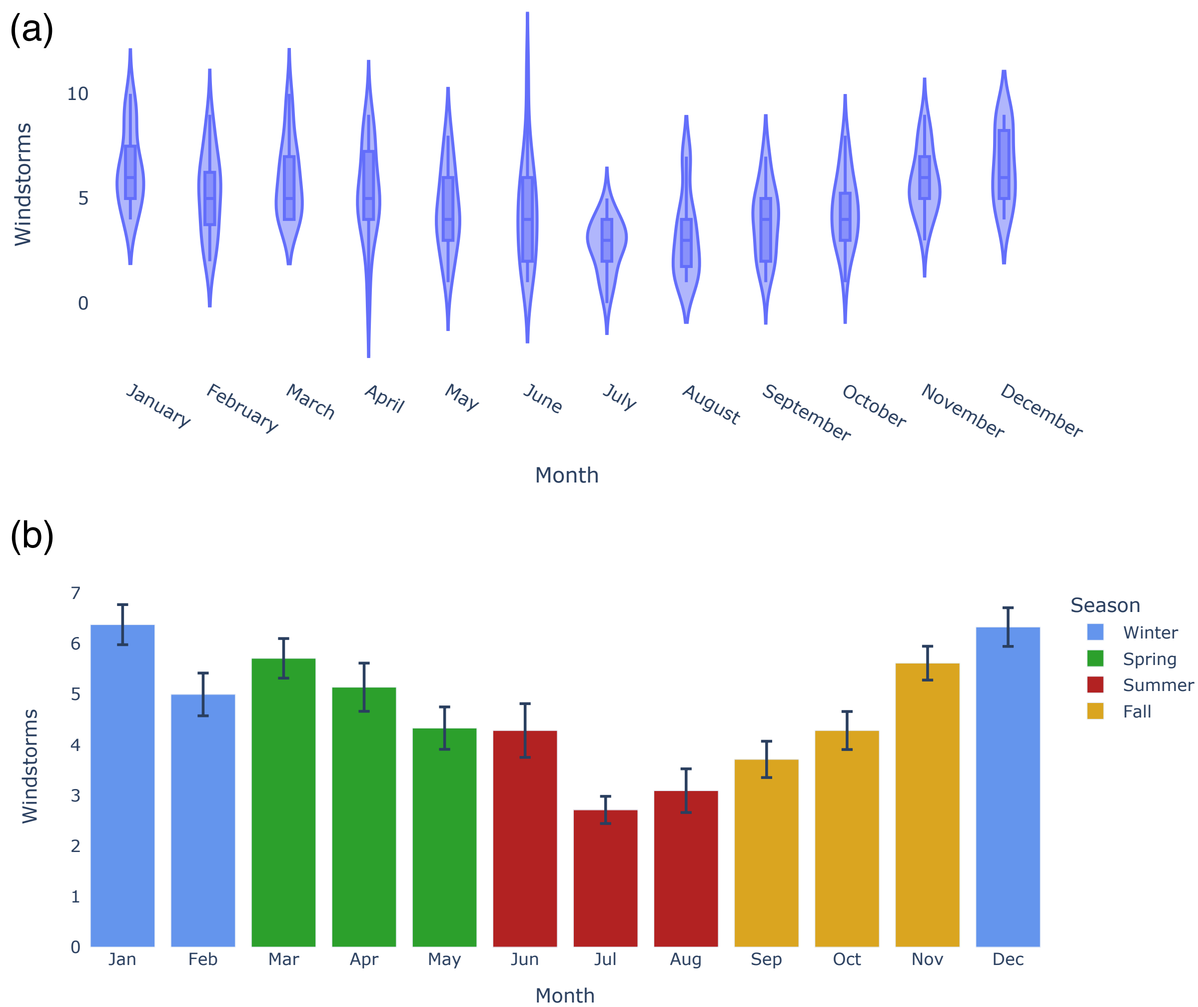

Figure 4.4: Monthly windstorm frequency distribution. (a) Violin plot showing distribution of windstorms for each month; (b) Bar plot showing average monthly windstorms with standard error along with seasonal trends.

To test the robustness of a seasonal trend, we apply the chi-square goodness-of fit test to test whether this data could have come from a uniform distribution. Applying the chi-square test to monthly DW counts results in a p-value of $p = 5.5e - 11$, thus providing justification to reject the null hypothesis that monthly windstorm counts are uniformly distributed. Additionally, windstorms and their properties are tested for significant differences using the paired t-test. As

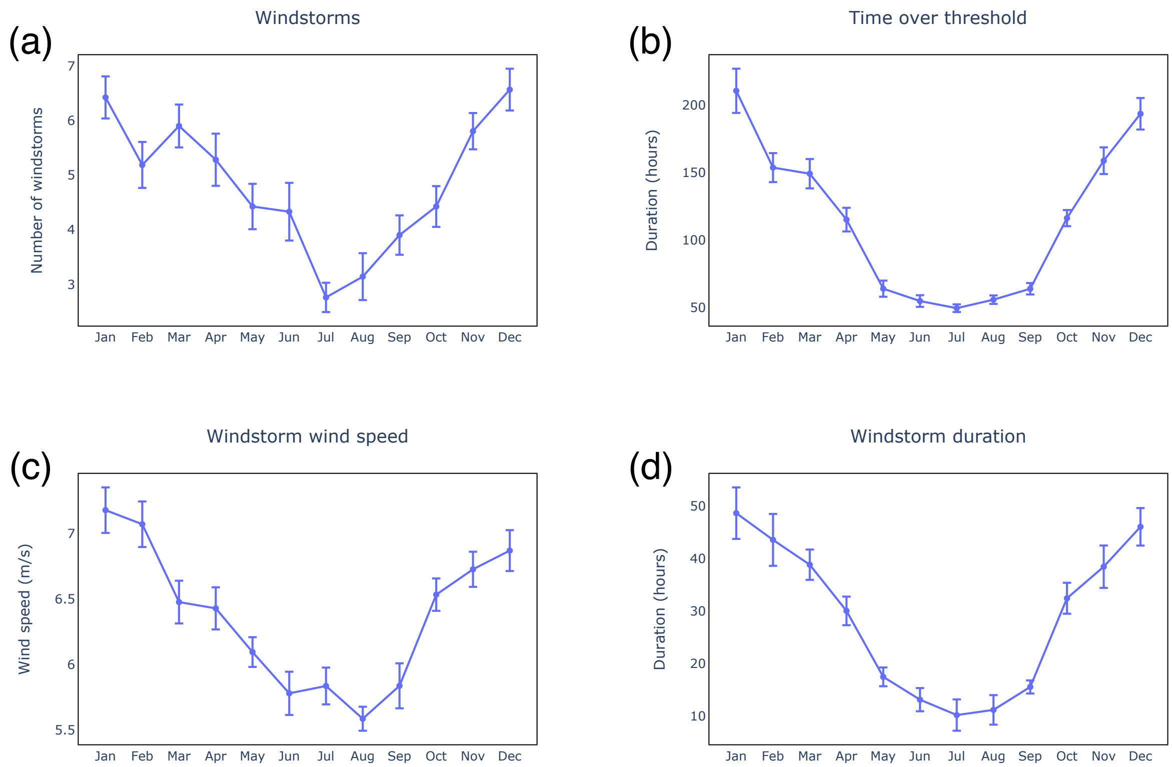

Figure 4.5: Seasonal trends using monthly data points. Error bars are computed via bootstrapping standard error. (a) Windstorm frequency represents the average number of monthly storms per year; (b) Time over threshold represents the average number of monthly hours of strong westerly winds per year; (c) Windstorm wind speeds represent the mean average wind speed during a windstorm in each month; (d) Windstorm durations represent the mean average windstorm duration in each month.

seen in Table 4.1, windstorm frequency, duration, wind speed and total hours of strong westerly winds significantly differ in the winter and summer months. These tests allow us to conclude the existence of a significant seasonal cycle in windstorm frequency, intensity and duration.

As depicted in Figure 4.5, the seasonal variance is high for windstorm frequencies, wind speeds, durations, and time spent over threshold, indicating strong seasonal trends for each of these parameters. Figure 4.6 illustrates the similarity in trends of monthly windstorm frequency compared with total hours of strong westerly winds, indicating that these parameters behave similarly within the annual cycle. Windstorm frequency computed monthly is additionally decomposed additively to observe the trend disregarding seasonality and interpolated over the full time period (Figure

	DW Frequency	DW Duration	DW Wind Speed	Time Over Threshold
Mean	$6.06, 3.41$	$45.15, 13.17$ (hours)	$7.04, 5.73$ (ms^{-1})	$186.11, 53.36$ (hours)
SD	$1.93, 2.04$	$19.21, 12.22$ (hours)	$0.78, 0.63$ (ms^{-1})	$64.87, 16.41$ (hours)
t	9.53	11.27	10.08	16.4
p	$9.33e-14$	$1.5e-16$	$1.3e-14$	$3.1e-24$

Table 4.1: Differences by the paired t-test between winter and summer downslope windstorm frequency, mean duration and mean wind speed, and total hours of strong westerly winds. Mean and SD are given as winter, summer.

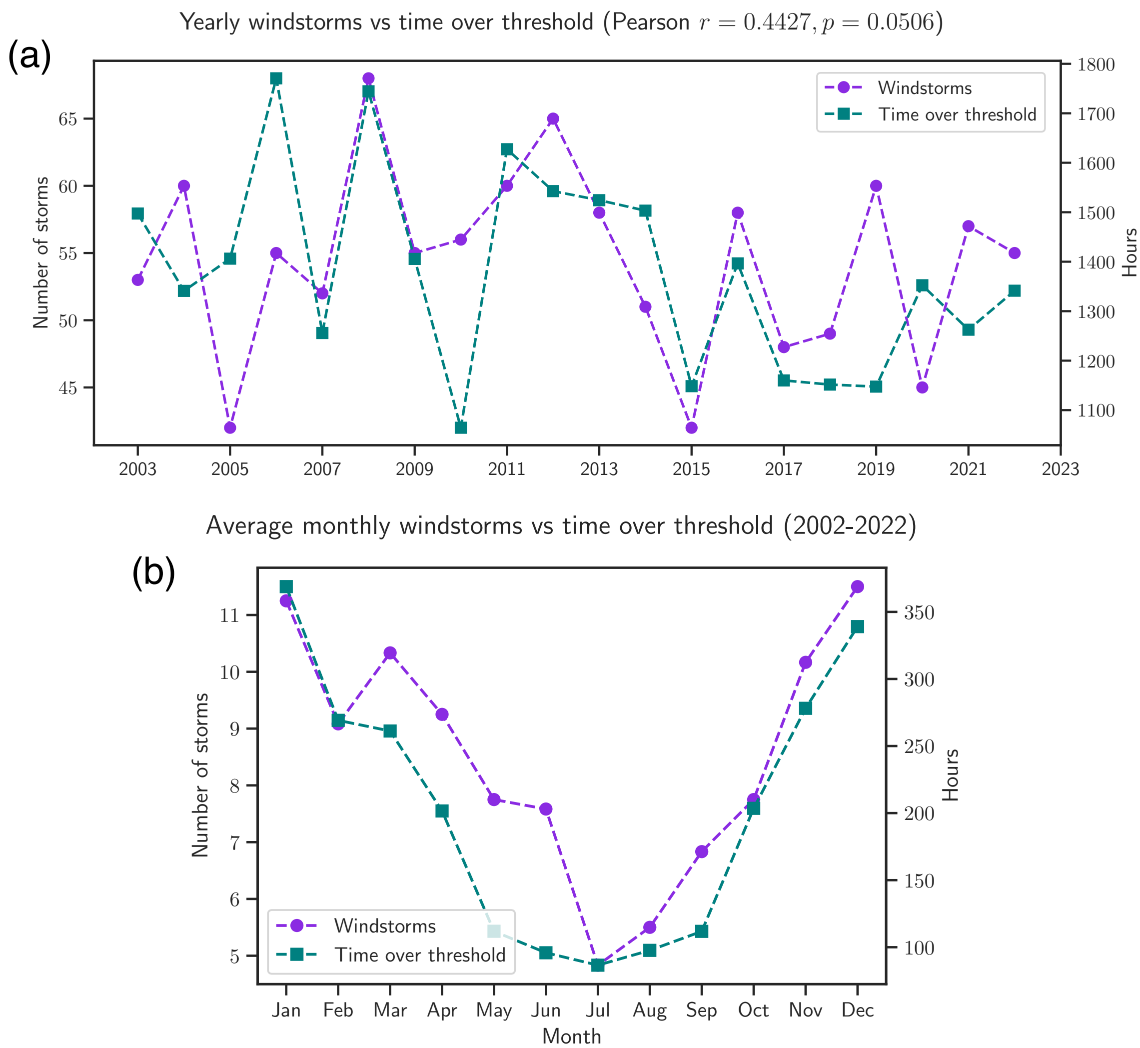

Figure 4.6: (a) Annual and (b) seasonal comparisons of windstorm frequency and time over threshold.

4.7). The smoothed function overlaid with the observed monthly windstorm frequency can be seen in Figure 4.8.

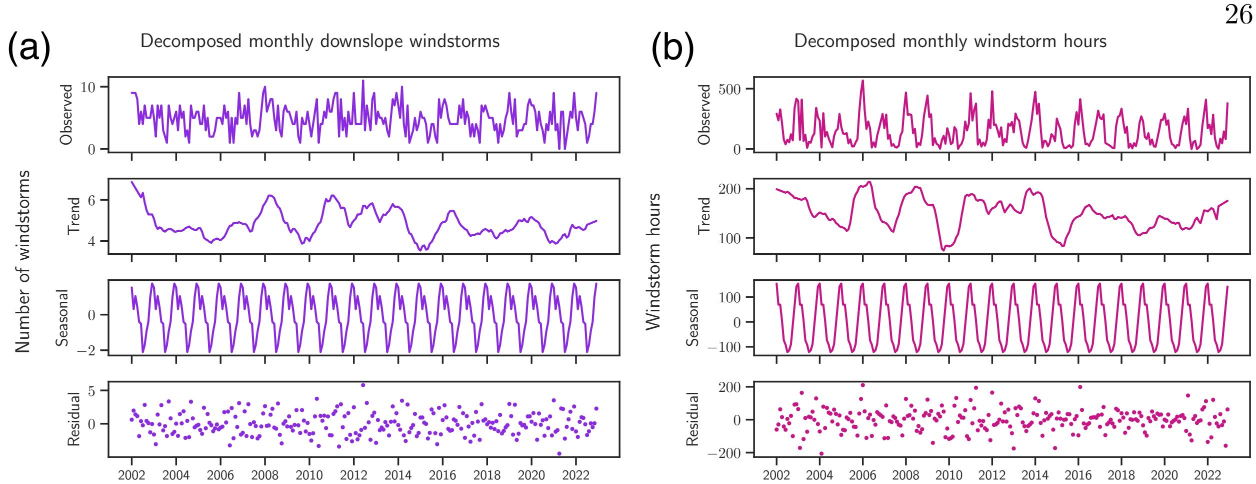

Figure 4.7: Decomposed monthly trends for (a) windstorm frequency and (b) windstorm hours interpolated with monthly data points. Generated via *seasonal_decompose* from the statsmodels package.

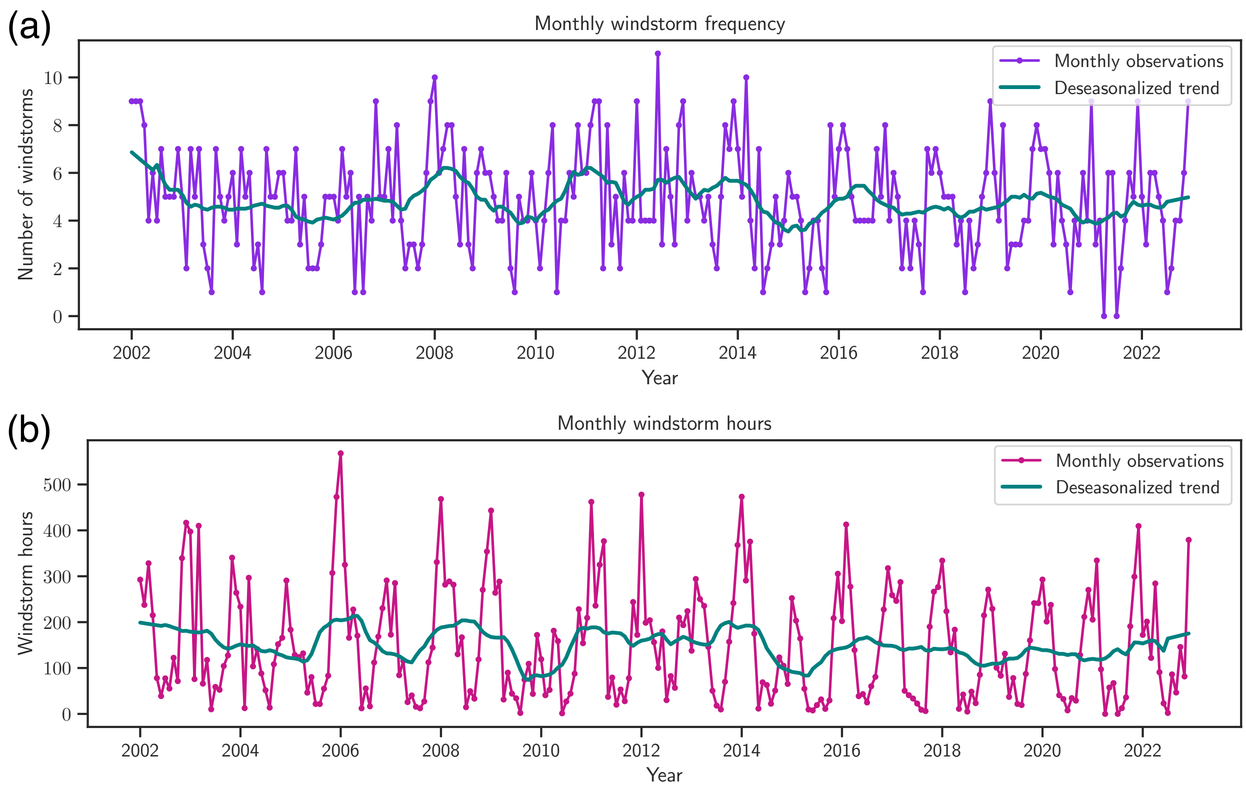

Figure 4.8: (a) Monthly windstorm frequency and (b) monthly windstorm hours overlaid with deseasonalized smoothed filter functions. By applying a moving-window convolutional filter with a frequency of 12, we effectively disregard the seasonal cycle to infer an interpolated underlying trend, plotted in teal.

4.3 Diurnal trends

No strong diurnal trend emerges for the occurrence of windstorms. Windstorm times overall appear to be roughly uniformly distributed, with a small peak in the late afternoon (Figure 4.9). Windstorm start times occur primarily during early- to mid- afternoon, and windstorm end times tend to be more spread, with most windstorms ending in the late evening. Heights of the bars in figure 4.9 represent the probability that a windstorm would start or end at a time spanned by each bar for the first two plots. For the third, heights represent the probability that a windstorm minute would occur at a time spanned by each bar.

4.4 MERRA-2 reanalysis comparison

Hourly wind speed data was used for both observations and reanalysis data to identify windstorm events to compare from both datasets. The paired t-test is used to test whether the mean difference between two sets of observations is zero. Annual DW frequency does not significantly differ by this test, with a test statistic $t = 1.76$ and an associated p=value of $p = 0.095$. In contrast, annual DW hours do significantly differ by the paired t-test, with a test statistic $t = 6.73$ and an associated p=value of $p = 2.6e - 06$. DW average wind speeds and durations differ significantly as well, with test statistics $t = 29.17$, $t = 3.52$ and corresponding p-values of $p = 1.3e - 16$, $p = 0.002$, respectively. Strong positive correlations are significant for annual DW hours, mean DW wind speed and mean DW duration, indicating that the MERRA2 reanalysis data performs adequately in capturing behavior in the winds associated with downslope windstorms. Notably, the wind speeds generated with MERRA-2 are much weaker than those observed, however similar annual DW frequencies are identified through both datasets.

To summarize, we have investigated trends of downslope windstorms and their properties at annual, seasonal, monthly and diurnal timescales. This revealed that downslope windstorms exhibit strong seasonal patterns, with higher frequencies, intensity, and duration in the winter months than the summer months. Windstorms are subject to high levels of variability from year

Figure 4.9: Diurnal distributions of (a) windstorm start times, (b) end times, and (c) overall windstorm temporal distribution. Heights are computed as probability values.

to year, which makes drawing conclusions regarding annual trends difficult. Time was not found to be a significant predictor of downslope windstorms through GLS or GLM regression models. The winds that comprise windstorms however were found to be significantly decreasing at a linear rate of 14 hours per year during the period 2002-2022. Additionally, 90th, 95th and 99th percentile

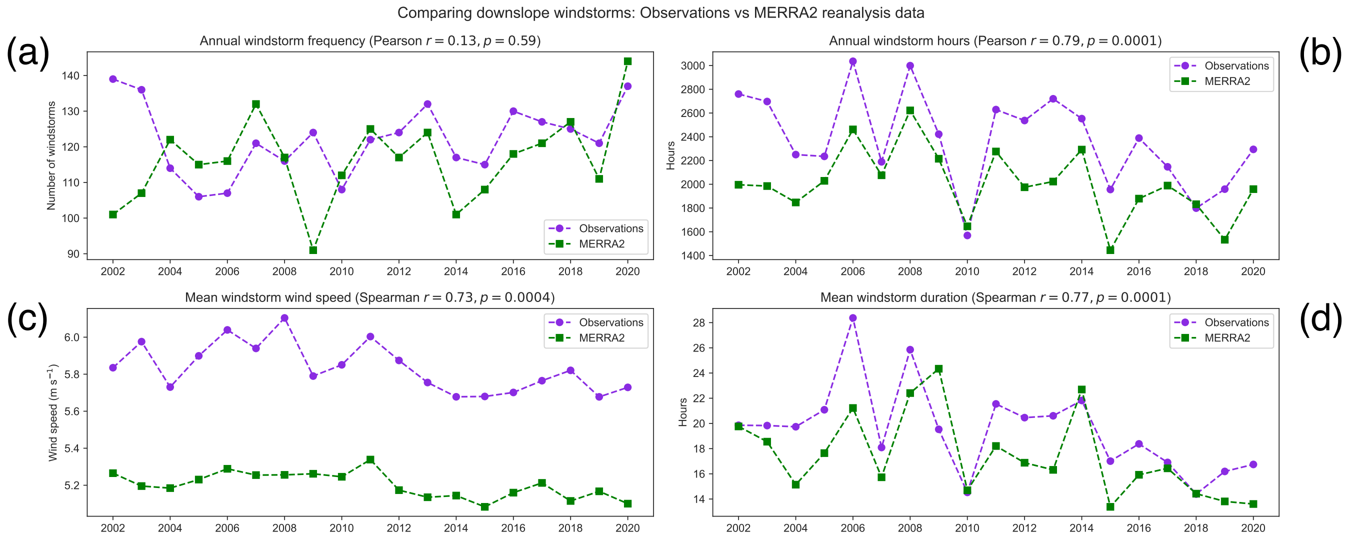

Figure 4.10: Comparison of results using observations and MERRA-2 reanalysis data for (a) DW frequency, (b) DW hours; (c) mean DW wind speed; and (d) mean DW duration. Correlations are assessed with Pearson's r for (a) and (b) whereas (c) and (d) are assessed with Spearman's r.

1-minute wind speeds were found to exhibit significant negative trends over this period as well, indicating that extreme wind events in the Front Range have decreased.

Chapter 5

Discussion

Over the period 2002 to 2022, 1170 downslope windstorm events were identified, averaging 55.7 windstorms per year with a standard deviation of 8.7 windstorms per year. Downslope windstorms exhibit notable variance from year to year, agreeing with previous studies [4, 40]. When analyzed on a monthly basis, the variance to mean ratio is significantly higher, with a mean of 4.8 windstorms per month and a standard deviation of 2.2 windstorms. This indicates that there is high variability of windstorms within a year, although the monthly windstorm counts over the 21 year period indicate a significant seasonal cycle.

While we did not conclude time to be a significant predictor of annual downslope windstorm events, we found a significant negative trend in annual hours of strong westerly winds. A decrease in annual windstorms has been observed in other locations, e.g. the Netherlands [12], across Europe [13], Russia [36] and Korea [37]. There are likely many factors that influence the change in annual windstorm frequency over time, and several studies have worked to create models for downslope windstorm events, e.g. [8, 24, 27]. We have additionally found decreases in extreme winds in Colorado's Front Range which agrees with some findings on extreme wind in the continental US. Ma et al. predicted a 20% reduction for the 99th percentile high wind frequency using CMIP5 for 2006–2098 [21], and Pryor et al. found statistically significant declines in 50th and 90th percentile and annual mean wind speeds based on two National Climate Data Center (NCDC) datasets from 1973-2005 [31].

Chapter 6

Conclusion

By analyzing a 21-year dataset of observed winds from the Front Range of the Rocky Mountains in North America, we assess the variable nature of windstorms. Downslope windstorms preferentially occur in the winter and spring and can occur at any time of day, though they are more likely to begin in the mid-afternoon and end in the late-afternoon and evening hours.

We identified downslope windstorm events based upon wind speed and wind direction meteorological data between 2002 and 2022 and assessed annual trends through generalized least squares and generalized linear models. Statistically significant decreases emerge in the number of strong westerly wind hours in the Boulder area. Additionally, extreme sustained winds at the 90th, 95th and 99th percentile wind speeds were found to be significantly decreasing during this period. When compared with windstorms classified using MERRA-2 reanalysis data, strong correlative annual trends are observed in total DW hours, DW intensity and DW duration, while similar annual DW frequencies are observed in both datasets. This indicates that the MERRA-2 reanalysis data has successfully captured DW trends in the Boulder area during this period.

There have been some limitations to this study. This climatology encompasses data from only one location, though the methodologies may be applied to data from any location. One other potential area of improvement is implementing a more advanced decomposition technique to separate the data into its overall trend, seasonal and residual components. The model used here would not capture, for example, shifting seasonal trends, as the seasonal component is calculated as the 12-month average of the detrended series.

In conclusion, our analysis of downslope windstorms has provided new recent insights into the frequency, duration and intensity of these storms between 2002 and 2022. Our findings suggest that windstorm activity and extreme winds are decreasing in the Front Range. The results of this study can inform the development of risk management strategies and mitigation efforts to protect communities from the impacts of windstorms by helping to improve downslope windstorm forecasting in the future. We hope that this research will not only provide a means to classify windstorms and analyze their changes over time, but also inspire further investigation into the causes and consequences of windstorms, and ultimately contribute to a better understanding of these extreme weather events.

Bibliography

[1] John T Abatzoglou, Benjamin J Hatchett, Paul Fox-Hughes, Alexander Gershunov, and Nicholas J Nauslar. Global climatology of synoptically-forced downslope winds. International Journal of Climatology, 41(1):31–50, 2021.

[2] William R Bergen and Allan H Murphy. Potential economic and social value of short-range forecasts of boulder windstorms. Bulletin of the American Meteorological Society, 59(1):29–44, 1978.

[3] GJ Bowden, Joan Adler, T Dabbs, and J Walter. The potential of wind energy in antarctica. Wind Engineering, pages 163–176, 1980.

[4] Waltraud Augusta Rosalie Brinkmann. A climatological study of strong downslope winds in the Boulder area. University of Colorado at Boulder, 1973.

[5] A Colin Cameron and Pravin K Trivedi. Regression-based tests for overdispersion in the poisson model. Journal of econometrics, 46(3):347–364, 1990.

[6] Yang Cao and Robert G Fovell. Downslope windstorms of san diego county. part i: a case study. Monthly Weather Review, 144(2):529–552, 2016.

[7] Stanley A Changnon. Temporal and spatial distributions of wind storm damages in the united states. Climatic Change, 94(3):473–482, 2009.

[8] Terry L Clark and RD Farley. Severe downslope windstorm calculations in two and three spatial dimensions using anelastic interactive grid nesting: A possible mechanism for gustiness. Journal of the Atmospheric Sciences, 41(3):329–350, 1984.

[9] Terry L Clark, William D Hall, Robert M Kerr, Don Middleton, Larry Radke, F Martin Ralph, Paul J Neiman, and David Levinson. Origins of aircraft-damaging clear-air turbulence during the 9 december 1992 colorado downslope windstorm: Numerical simulations and comparison with observations. Journal of the atmospheric sciences, 57(8):1105–1131, 2000.

[10] Andrew Clifton and Julie K. Lundquist. Data Clustering Reveals Climate Impacts on Local Wind Phenomena. Journal of Applied Meteorology and Climatology, 51(8):1547–1557, March 2012.

[11] Andrew Clifton, Scott Schreck, George Scott, Neil Kelley, and Julie K Lundquist. Turbine inflow characterization at the national wind technology center. Journal of solar energy engineering, 135(3), 2013.

[12] Stephen Cusack. A 101 year record of windstorms in the netherlands. Climatic Change, 116(3):693–704, 2013.

[13] Laura C Dawkins, David B Stephenson, Julia F Lockwood, and Paul E Maisey. The 21st century decline in damaging european windstorms. Natural Hazards and Earth System Sciences, 16(8):1999–2007, 2016.

[14] Dale R Durran. Downslope winds. Encyclopedia of atmospheric sciences, 644:650, 2003.

[15] William Gardner, Edward P Mulvey, and Esther C Shaw. Regression analyses of counts and rates: Poisson, overdispersed poisson, and negative binomial models. Psychological bulletin, 118(3):392, 1995.

[16] Branko Grisogono and Danijel BelusŠIĆ. A review of recent advances in understanding the mesoand microscale properties of the severe bora wind. Tellus A: Dynamic Meteorology and Oceanography, 61(1):1–16, 2009.

[17] Noriszura Ismail and Abdul Aziz Jemain. Handling overdispersion with negative binomial and generalized poisson regression models. In Casualty actuarial society forum, volume 2007, pages 103–58. Citeseer, 2007.

[18] David Kahle and Hadley Wickham. ggmap: Spatial visualization with ggplot2. The R Journal, 5(1):144–161, 2013.

[19] JB Klemp and DR Lilly. The dynamics of wave-induced downslope winds. Journal of Atmospheric Sciences, 32(2):320–339, 1975.

[20] Douglas K Lilly. A severe downslope windstorm and aircraft turbulence event induced by a mountain wave. Journal of Atmospheric Sciences, 35(1):59–77, 1978.

[21] Chen-Geng Ma and Edmund KM Chang. Impacts of storm-track variations on wintertime extreme weather events over the continental united states. Journal of Climate, 30(12):4601–4624, 2017.

[22] Richard F Madole, William C Bradley, Deborah S Loewenherz, Dale F Ritter, Nathaniel W Rutter, and Colin E Thorn. Rocky mountains. Geological Society of America, Inc., 1987.

[23] Clifford F Mass and David Ovens. The northern california wildfires of 8–9 october 2017: The role of a major downslope wind event. Bulletin of the American Meteorological Society, 100(2):235–256, 2019.

[24] Andrew E Mercer, Michael B Richman, Howard B Bluestein, and John M Brown. Statistical modeling of downslope windstorms in boulder, colorado. Weather and forecasting, 23(6):1176–1194, 2008.

[25] GMAO MERRA. tavg1_2d_slv_nx: 2d, 1-hourly, time-averaged, single-level, assimilation, single-level diagnostics v5. 12.4. 2015, 2.

[26] Chipo Mufudza and Hamza Erol. Poisson mixture regression models for heart disease prediction. Computational and Mathematical Methods in Medicine, 2016, 2016.

[27] Louisa B Nance and Bradley R Colman. Evaluating the use of a nonlinear two-dimensional model in downslope windstorm forecasts. Weather and forecasting, 15(6):715–729, 2000.

[28] Federico Augusto Norte. Understanding and forecasting zonda wind (andean foehn) in argentina: a review. Atmospheric and Climate Sciences, 5(3):163–193, 2015.

[29] Michael J Oard. A method for predicting chinook winds east of the montana rockies. Weather and forecasting, 8(2):166–180, 1993.

[30] Stefan Pfenninger and Iain Staffell. Long-term patterns of european pv output using 30 years of validated hourly reanalysis and satellite data. Energy, 114:1251–1265, 2016.

[31] SC Pryor, RJ Barthelmie, DT Young, ES Takle, RW Arritt, David Flory, WJ Gutowski Jr, A Nunes, and J Roads. Wind speed trends over the contiguous united states. Journal of Geophysical Research: Atmospheres, 114(D14), 2009.

[32] F Martin Ralph, Paul J Neiman, and David Levinson. Lidar observations of a breaking mountain wave associated with extreme turbulence. Geophysical research letters, 24(6):663–666, 1997.

[33] MN Raphael. The santa ana winds of california. Earth Interactions, 7(8):1–13, 2003.

[34] Hans Richner and Patrick Hächler. Understanding and forecasting alpine foehn. Mountain Weather Research and Forecasting: Recent Progress and Current Challenges, pages 219–260, 2013.

[35] Scott M Robeson and Karsten A Shein. Spatial coherence and decay of wind speed and power in the north-central united states. Physical Geography, 18(6):479–495, 1997.

[36] Anna A Shestakova, Pavel A Toropov, and Tatiana A Matveeva. Climatology of extreme downslope windstorms in the russian arctic. Weather and Climate Extremes, 28:100256, 2020.

[37] Yewon Shin, Jung-Hoon Kim, Hye-Yeong Chun, Wook Jang, and Seok-Woo Son. Classification of synoptic patterns with mesoscale mechanisms for downslope windstorms in korea using a self-organizing map. Journal of Geophysical Research: Atmospheres, 127(6):e2021JD035867, 2022.

[38] Iain Staffell and Stefan Pfenninger. Using bias-corrected reanalysis to simulate current and future wind power output. Energy, 114:1224–1239, 2016.

[39] Anthony L Westerling, Daniel R Cayan, Timothy J Brown, Beth L Hall, and Laurence G Riddle. Climate, santa ana winds and autumn wildfires in southern california. Eos, Transactions American Geophysical Union, 85(31):289–296, 2004.

[40] C David Whiteman and Johanna G Whiteman. An historical climatology of damaging downslope windstorms at Boulder, Colorado, volume 55. Environmental Research Laboratories, 1974.